Electronic Supplementary Material (ESI) for Chemical Science.

Supporting information

Non-redox doping boosts oxygen evolution electrocatalysis on hematite

Huu Chuong Nguyën,[a‡] Felipe Andrés Garcés-Pineda,[a‡] Mabel de Fez-Febré,[a,b] José Ramón Galán-Mascarós,*[a,c] and Núria López*[a]

[a] *Institute of Chemical Research of Catalonia (ICIQ), The Barcelona Institute of Science and Technology, Av. Països Catalans 16, Tarragona 43007, Spain; E-mail: jrgalan@iciq.es; nlopez@iciq.es*
[b] *Departament de Quimica Fisica i Inorganica, Universitat Rovira i Virgili, Marcel.lí Domingo s/n, Tarragona, E-43007, Spain.*
[c] *ICREA, Passeig Lluis Companys, 23 , Barcelona 08010,Spain.*

Additional experimental details

TOF estimation

Turn over frequency was estimated from the ratio between moles of oxygen, calculated from current density data, and the moles of active sites on the electrode. To estimate the total number of active sites, we followed a literature procedure.[1] This procedure relates the concentration of redox active centres from the slope in the linear relationship between the peak current of a pre-catalytic reversible redox wave (around 1.45 V vs RHE in this case) and scan rate from the equation:

$$i = \frac{n^2F^2VAC_a\upsilon}{4RT} \tag{1}$$

where $n = 1$; F = Faraday's constant; A = electrode surface area; C_a = surface concentration of active sites; υ = scan rate; R = ideal gas constant; T = temperature. The results of this estimation are shown in Figure S23.

Binding energy measurements

Binding energy were evaluated following a method previously described.[2] To estimate the free energy of formation of *OH and *O, we examined the potentials of *OH (acidic: $^*H_2O \rightarrow {}^*OH + H^+ + e^-$; alkaline: $^*H_2O + OH^- \rightarrow {}^*OH + H_2O + e^-$) and *O (acidic: $^*OH \rightarrow {}^*O + H^+ + e^-$; alkaline: $^*OH + OH^- \rightarrow {}^*O + H_2O + e^-$). The electrochemical potentials of OHad ($\Delta G_{*OH} = V_{peak}1$) and *O ($\Delta G_{*O} = V_{peak}1 + V_{peak}2$) correspond to the free energies of $^*H_2O \rightarrow {}^*OH + 1/2\ H_2$ and $^*H_2O \rightarrow {}^*O + H_2$, respectively.

Additional computational details

Group symmetry

We looked for the possible ways to dope the hematite in a (2×2) supercell with the symmetry space group 167 (R-3c) using the software made by Dr Ricardo Grau-Crespo.[3] We obtained 19 non-equivalent configurations for substituting two Zn atoms in Fe_2O_3 (5% doping) and 1466 non-equivalent configurations for substituting four Zn atoms in Fe_2O_3 (10% doping). By imposing central symmetry to have a symmetric surface on both surfaces of the bulk we have only 15 non-equivalent configurations for substituting four Zn atoms in Fe_2O_3 (10% doping).

Electron density difference

Electron density were computed with VASP 5.4.4[4] with an energy cut-off of 700 eV with PAW pseudopotential. The electron density difference $\Delta\rho$ was computed following:

$$\Delta\rho = \rho_{tot} - \rho_{\mathrm{H_3O}} - \rho_{surf} \tag{2}$$

where ρ_{tot} is the electron density of the full system, $\rho_{\mathrm{H_3O}}$ is the electron density of the H_3O and ρ_{surf} is the electron density of the surface.

Computational Hydrogen Electrode model

We assume water oxidation mechanism following series of proton-coupled electron transfer (PCET) steps.[5–11] To calculate the free energy, we use the method developed by Nørskov et al.[11] The derivation of the model and the required approximations within standard DFT were implemented as follows.

The computational standard hydrogen electrode (SHE), $1/2\ H_2 \rightleftharpoons H^+ + e^-$ at $p_{\mathrm{H_2}} = 1$ bar and $T = 298$ K, is set to be the reference potential. We are interested in its relationship with the chemical potential of protons and electrons. By definition an electrode potential is $U = 0$. For a PCET we do not need to know the chemical potentials of electrons and protons separately, using the SHE as reference their sum can be taken to be equal to the chemical potential of gas phase hydrogen. At standard conditions ($U_b = 0$, pH 0 , p = 1 bar, T = 298 K), the reaction free energy ΔG_r of $HA^* \rightarrow A + H^+ + e^-$ can be calculated as that of $HA^* \rightarrow A + 1/2\ H_2$. In other terms, we assume the hydrogen electrode to be in equilibrium, i.e. the solvated protons and electrons are in equilibrium with the hydrogen in the gas phase:

$$H^+(aq) + e^- \rightleftharpoons \frac{1}{2}H_2(g)$$

In terms of chemical potentials the equilibrium is expressed as

$$\mu_{H^+} + \mu_{e^-} = \frac{1}{2}\mu_{H_2(g)} \tag{3}$$

This relation can be developed in

$$\mu_{H^+} = \mu^0_{H^+} + k_B T \ln a_{H^+} \tag{4}$$

$$\mu_{e^-} = \mu^0_{e^-} - eU \tag{5}$$

$$\mu_{H_2(g)} = \mu^0_{H_2} + k_B T \ln p_{H_2} \tag{6}$$

where a_{H^+} represents the activity of the protons. It is related to the pH. The effect of pH is to modify the chemical potential of protons by $-k_b T \ln(10)$pH. eU represents the shift in electron energy when a bias is applied. The effect of an external potential U_{ext} measured against the SHE is to modify the chemical potential of the electrons by $-eU_{ext}$, and $p_{H_2}$is the partial pressure of hydrogen. $\mu^0_{H^+}, \mu^0_{e^-}, \mu^0_{H_2(g)}$ are the chemical potential of protons, electrons and hydrogen, respectively, at standard conditions ($p_{H_2} = 1$ bar, $a_{H^+} = 1$, T = 298.15 K). At the standard conditions, we have naturally

$$\mu^0_{H^+} + \mu^0_{e^-} = \frac{1}{2}\mu^0_{H_2(g)} \tag{7}$$

From a computational point of view the chemical potential of hydrogen in the gas phase is much easier to calculate than the chemical potential of protons. The chemical potential μ is a Gibbs' free energy (G) while the Kohn-Sham energy(E_{DFT}) + the zero-point energy (ZPE) correction correspond to an enthalpy (H). They are related via the equation below:

$$G(T,p) = H(T,p) - TS(T,p) \tag{8}$$

Where S is the entropy of the system, or entropy contribution, calculated using ideal gas approximation taking into account the translational and rotational vibrations:

$$S = k_B \ln \prod_{i=1}^{N} \frac{1}{1 - \exp(\hbar\omega_{X,i}/k_B T)} \tag{9}$$

We can therefore estimate the reaction free energy of a PCET as

$$\Delta G = \Delta H - T\Delta S - eU_{ext} + k_b T \cdot \ln(10) \cdot \mathrm{pH} \tag{10}$$

$$\Delta H = \Delta U_{trans} + \Delta U_{rot} + \Delta U_{vib} + \Delta(ZPE) + \Delta H_{elec} \tag{11}$$

$$\Delta S = \Delta S_{trans} + \Delta S_{rot} + \Delta S_{vib} \tag{12}$$

ZPE and entropic contributions to the free energy of *O, *OH, and *OOH do not change considerably from surface to surface of different metal oxides.[11] They are therefore transferable as first approximation. We can define the standard chemical potential of hydrogen on the DFT scale as:

$$\mu^0_{H_2(g)} = E^{H_2(g)}_{DFT} + ZPE_{H_2(g)} - TS^0_{H_2(g)} \tag{13}$$

Where $S^0$is the standard entropy of hydrogen and is taken from thermodynamic tables for gas-phase molecules. We also need another approximation to estimate the chemical potential of water in the liquid phase. At 0.035 bar, the chemical potential of liquid water is equal to the chemical potential of water in the gas phase at T = 298.15 K. At this pressure we can approximate

$$\mu_{\mathrm{H_2O}(l)} = \mu_{\mathrm{H_2O}(g)} \tag{14}$$

Using DFT, the potential of water in gas phase is described as follows:

$$\mu_{\mathrm{H_2O}(g)} = E_{DFT}^{H_2O(g)} + ZPE_{\mathrm{H_2O}} - TS^0_{\mathrm{H_2O}}(0.035\,\mathrm{bar}) \tag{15}$$

This approximation is required because of the difficulty to compute the exact hydrogen bond contribution to the total energy of water within standard DFT. Another required approximation comes from the difficulty to accurately compute the energy of the oxygen molecule with standard DFT.[12] We will use the experimental value of 2.46 V (or 1.23 eV per electron)[13] of the standard free energy change of the reaction

$$\mathrm{H_2O}(l) \rightleftharpoons \frac{1}{2}\mathrm{O_2}(g) + \mathrm{H_2}(g) \tag{16}$$

Which gives the useful relations:

$$\frac{1}{2}G^0_{\mathrm{O_2}(g)} + G^0_{\mathrm{H_2}(g)} - G^0_{\mathrm{H_2O}(l)} = 2.46\,\mathrm{eV} \tag{17}$$

$$G^0_{\mathrm{O_2}(g)} = 2\left(G^0_{\mathrm{H_2O}(l)} - G^0_{\mathrm{H_2}(g)}\right) + 4.92\,\mathrm{eV} \tag{18}$$

If we rewrite everything in terms of DFT energies, using Eq.(13) and Eq.(15) in Eq.(18), we can thereby approximate the free energy of an oxygen molecule in terms of the DFT energy of $\mathrm{H_2O}(g)$, $\mathrm{H_2}(g)$ as follows:

$$\begin{aligned}
G^0_{O_2(g)} &= E_{DFT}^{O_2(g)} + ZPE_{O_2(g)} - TS^0_{O_2(g)} && (19)\\
&= 2\left(E_{DFT}^{H_2O(g)} + ZPE_{H_2O(g)} - TS^0_{H_2O(g)} - E_{DFT}^{H_2(g)} - ZPE_{H_2(g)} + TS^0_{H_2(g)}\right) + 4.92\,\mathrm{eV} && (20)\\
&= 2\left(E_{DFT}^{H_2O(g)} + ZPE_{H_2O(g)} - TS^0_{H_2O(g)}\right) - 2\left(E_{DFT}^{H_2(g)} + ZPE_{H_2(g)} - TS^0_{H_2(g)}\right) + 4.92\,\mathrm{eV} && (21)
\end{aligned}$$

The universal (single site) OER on oxide surfaces can be extracted from reference 14. Thus, we consider a four-step reaction path in OER for which we can compute the free energy for each. The first step is water splitting on the active site with a release of a proton and an electron:

$$\mathrm{H_2O}(l) + * \rightleftharpoons {}^*\mathrm{OH} + \mathrm{H^+} + e^- \tag{22}$$

$$\Delta G_1 = G_{^*\mathrm{OH}} - G_{\mathrm{H_2O}(l)} - eU_{ext} + k_bT \cdot \ln(10) \cdot \mathrm{pH}$$

Let's derive ΔG_1 step-by-step. From Eq.(22), we can write:

$$\Delta G_1 = G_{\mathrm{OH}^*} + \mu_{\mathrm{H^+}} + \mu_{e^-} - G_* - \mu_{\mathrm{H_2O}(l)} \tag{23}$$

where G_{OH^*} and G_* are the free energies of the surface with and without OH* respectively. They can be rewritten in terms of DFT energies as:

$$G_{\mathrm{OH}^*} = E_{DFT}^{*\mathrm{OH}} + ZPE_{\mathrm{OH}^*} - TS^0_{\mathrm{OH}^*} \tag{24}$$

$$G_* = E^*_{DFT} \tag{25}$$

We have used the athermal limit approximation for the free energy of the slab and its temperature dependence is ignored as it is negligible compared to that of the gas. Using Eq.(4,5,14) in Eq.(23), we get:

$$\Delta G_1 = G_{*\mathrm{OH}} + \mu^0_{\mathrm{H}^+} + k_B T \ln a_{\mathrm{H}^+} + \mu^0_{e^-} - eU - G_* - \mu_{\mathrm{H_2O(g)}} \tag{26}$$

Further on, substituting Eq. (7,13,15,24,25) in Eq.(26), we obtain an expression of the reaction free energy based on the DFT energy scale:

$$\begin{aligned}\Delta G_1 =& E^{*\mathrm{OH}}_{DFT} - E^*_{DFT} + \frac{1}{2}E^{\mathrm{H_2(g)}}_{DFT} - E^{\mathrm{H_2O(g)}}_{DFT} + \left(ZPE_{*\mathrm{OH}} + \frac{1}{2}ZPE_{\mathrm{H_2(g)}} - ZPE_{\mathrm{H_2O(g)}}\right) \\ & - T\left(S^0_{*\mathrm{OH}} + \frac{1}{2}S^0_{\mathrm{H_2(g)}} - S^0_{\mathrm{H_2O(g)}}\right) - eU + k_B T \ln a_{\mathrm{H}^+}\end{aligned} \tag{27}$$

The second step of the reaction is oxidation of the OH* species to O* with release of a proton and an electron:

$$^*\mathrm{OH} \rightleftharpoons {}^*\mathrm{O} + \mathrm{H}^+ + e^- \tag{28}$$

$$\Delta G_2 = G_{*\mathrm{O}} - G_{*\mathrm{OH}} - eU_{ext} + k_b T \cdot \ln(10) \cdot \mathrm{pH}$$

The change in free energy for the forward reaction is

$$\Delta G_2 = G_{*\mathrm{O}} - G_{*\mathrm{OH}} + \mu_{\mathrm{H}^+} + \mu_{e^-} \tag{29}$$

where $G_{*\mathrm{O}}$ and $G_{*\mathrm{OH}}$ represent the free energies of the surface with *O and *OH adsorbed respectively. Replacing Eq.(4,5,7,13,24) in Eq.(29), we obtain

$$\begin{aligned}\Delta G_2 =& E^{*\mathrm{O}}_{DFT} - E^{*\mathrm{OH}}_{DFT} + \frac{1}{2}E^{\mathrm{H_2(g)}}_{DFT} + \left(ZPE_{*\mathrm{O}} - ZPE_{*\mathrm{OH}} + \frac{1}{2}ZPE_{\mathrm{H_2(g)}}\right) - T\left(S_{*\mathrm{O}} - S_{*\mathrm{OH}} + \frac{1}{2}S_{\mathrm{H_2}}\right) \\ & - eU + k_B T \ln a_{\mathrm{H}^+}\end{aligned} \tag{30}$$

The third step corresponds to the water splitting on top of oxygen:

$$^*\mathrm{O} + \mathrm{H_2O}(l) \rightleftharpoons {}^*\mathrm{OOH} + \mathrm{H}^+ + e^- \tag{31}$$

$$\Delta G_3 = G_{*\mathrm{OOH}} - G_{*\mathrm{O}} - eU_{ext} + k_b T \cdot \ln(10) \cdot \mathrm{pH}$$

The change in free energy for the forward reaction is

$$\Delta G_3 = G_{*\mathrm{OOH}} + \mu_{\mathrm{H}^+} + \mu_{e^-} - \mu_{\mathrm{H_2O(l)}} \tag{32}$$

Repeating the same steps as previously, we obtain

$$\begin{aligned}\Delta G_3 =& E^{*\mathrm{OOH}}_{DFT} + \frac{1}{2}E^{\mathrm{H_2(g)}}_{DFT} - E^{*\mathrm{O}}_{DFT} - E^{\mathrm{H_2O(g)}}_{DFT} + \left(ZPE_{*\mathrm{OOH}} + \frac{1}{2}ZPE_{\mathrm{H_2(g)}} - ZPE_{*\mathrm{O}} - ZPE_{\mathrm{H_2O(g)}}\right) \\ & - T\left(S^0_{*\mathrm{OOH}} + \frac{1}{2}S_{\mathrm{H}_2^0} - S^0_{*\mathrm{O}} - S^0_{\mathrm{H_2O(g)}}\right) - eU + k_B T \ln a_{\mathrm{H}^+}\end{aligned} \tag{33}$$

The last step is the evolution of oxygen:

$$^{*}\mathrm{OOH} \rightleftharpoons * + \mathrm{O}_2(g) + \mathrm{H}^+ + e^- \tag{34}$$

$$\Delta G_4 = G_{\mathrm{O}_2} - G_{^*\mathrm{OOH}} - eU_{ext} + k_b T \cdot \ln(10) \cdot \mathrm{pH}$$

The change in free energy for the forward reaction is

$$\Delta G_4 = G_* + G_{\mathrm{O_2(g)}} + \mu_{\mathrm{H}^+} + \mu_{e^-} - G_{^*\mathrm{OOH}} \tag{35}$$

Doing the same substitution as previously with Eq.(21) for $G_{\mathrm{O_2(g)}}$ in Eq.(35), we obtain

$$\begin{aligned}\Delta G_4 =& E^*_{DFT} + 2\left(E^{\mathrm{H_2O(g)}}_{DFT} + ZPE_{\mathrm{H_2O(g)}} - TS^0_{\mathrm{H_2O(g)}}\right) - 2\left(E^{\mathrm{H_2(g)}}_{DFT} - ZPE_{\mathrm{H_2(g)}} + TS^0_{\mathrm{H_2(g)}}\right) + 4.92\,\mathrm{eV} \\ &+ \frac{1}{2}\left(E^{\mathrm{H_2(g)}}_{DFT} - ZPE_{\mathrm{H_2(g)}} + TS^0_{\mathrm{H_2(g)}}\right) + k_B T \ln a_{\mathrm{H}^+} - eU - E^{^*\mathrm{OOH}}_{DFT} - ZPE_{^*\mathrm{OOH}} + TS^0_{^*\mathrm{OOH}}\end{aligned} \tag{36}$$

$$\begin{aligned}\Delta G_4 =& E^*_{DFT} + 2E^{\mathrm{H_2O(g)}}_{DFT} - E^{^*\mathrm{OOH}}_{DFT} - \frac{3}{2}E^{\mathrm{H_2(g)}}_{DFT} + \left(2ZPE_{\mathrm{H_2O(g)}} - ZPE_{^*\mathrm{OOH}} - \frac{3}{2}ZPE_{\mathrm{H_2(g)}}\right) \\ &- T\left(2S^0_{\mathrm{H_2O(g)}} - S^0_{^*\mathrm{OOH}} - \frac{3}{2}S^0_{\mathrm{H_2(g)}}\right) + k_B T \ln a_{\mathrm{H}^+} - eU + 4.92\,\mathrm{eV}\end{aligned} \tag{37}$$

or alternatively if you keep Eq.(21) for $G_{\mathrm{O_2(g)}}$:

$$\begin{aligned}\Delta G_4 =& E^*_{DFT} - E^{^*\mathrm{OOH}}_{DFT} + \frac{1}{2}E^{\mathrm{H_2(g)}}_{DFT} + G_{\mathrm{O_2(g)}} + \left(-ZPE_{^*\mathrm{OOH}} + \frac{1}{2}ZPE_{\mathrm{H_2(g)}}\right) \\ &- T\left(-S^0_{^*\mathrm{OOH}} + \frac{1}{2}S^0_{\mathrm{H_2(g)}}\right) + k_B T \ln a_{\mathrm{H}^+} - eU\end{aligned} \tag{38}$$

The potential determining step is the one with the largest ΔG:

$$G^{\mathrm{OER}} = \max\left[\Delta G_1, \Delta G_2, \Delta G_3, \Delta G_4\right] \tag{39}$$

at $U = 0$ V, pH 0 and $T = 298.15$ K. The theoretical overpotential (independent of the pH), at standard conditions is given by

$$\eta^{\mathrm{OER}} = \left(\frac{G^{\mathrm{OER}}}{e}\right) - 1.23\,\mathrm{V} \tag{40}$$

We used symmetric slabs to avoid some unphysical numerical artifacts that come from modeling a slab in a periodic system with full geometry optimisation on both sides. Our E_{DFT} contains two adsorbed molecules instead of one. To take that into account we assumed

$$E^{^*\mathrm{O}}_{DFT} - E^*_{DFT} = \frac{1}{2}\left(E^{2^*\mathrm{O}}_{DFT} - E^*_{DFT}\right) \tag{41}$$

We can therefore write:

$$E^{^*\mathrm{O}}_{DFT} = \frac{1}{2}\left(E^{2^*\mathrm{O}}_{DFT} - E^*_{DFT}\right) + E^*_{DFT} \tag{42}$$

For n (even) times species X, we generalize that to

$$E^{X^*}_{DFT} = \frac{1}{n}\left(E^{nX^*}_{DFT} - E^*_{DFT}\right) + E^*_{DFT} \tag{43}$$

2D random walk for PCET

For a memoryless random walk (or Bernoulli process), the diffusion coefficient for a d-dimensional random walk is given by the Einstein relation[15]:

$$2dDt = \left\langle x^2 \right\rangle \tag{44}$$

where $\left\langle x^2 \right\rangle$ is the mean squared displacement.

We will restrict ourself to a 2-dimensional discrete random walk where each jump has a displacement l and a duration τ. The total displacement is therefore $x = nł$ and the total time is $t = n\tau$ where n is the number of jumps. It is trivial to show that in this case the diffusion coefficient is

$$D = \frac{l^2}{4\tau} \tag{45}$$

We can approximate l from the actual distance between Zn and Fe site: $l \approx 5.14$ Å. The jumping time can be approximated by the frequency of PCET obtained from DFT: 19.40411 THz. Thus, $\tau = 1/f \approx 50$ fs.

Application of the 2D random walk to PCET to Fe_2O_3

If we suppose a homogeneous coverage of Zn atoms and the rest are Fe atoms on the surface. For a surface of 10 × 10 sites, with a 10% doping of Zn, we would have 10 Zn sites and 90 Fe sites. Since the coverage is homogeneous, it is equivalent to cut a single row of one Zn and nine Fe centers and multiply it by 10. One can start on this one-dimensional system for the sake of simplicity. We want to estimate the expectation time before an H atom reaches a Zn site. If p is the coverage ratio (p = 1/10) and the maximal size of the row is m we can write more generally, the expectation time as

$$E(t) = \sum_{i=0}^{m} E(t|n=i) = \sum_{n=0}^{m} n \binom{n}{k} p^k (1-p)^{n-k} \tau = mp\tau \tag{46}$$

Since this is a Bernoulli process that follows a binomial distribution, we have shown that the expectation time increases linearly with the size and therefore the current must decrease linearly too.

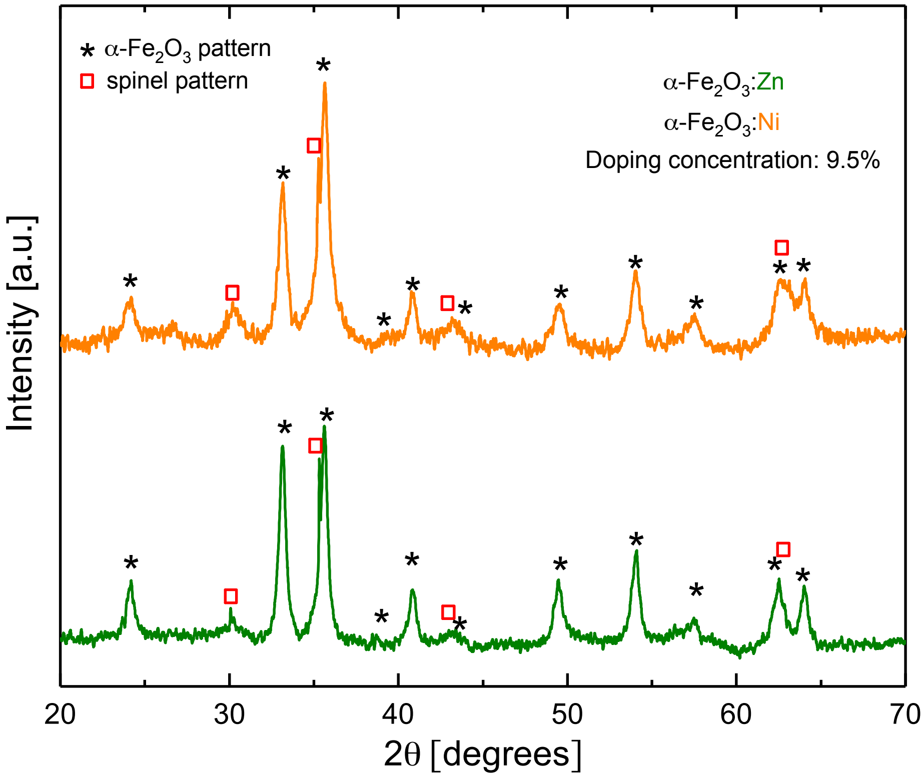

Figure S1 ***S*1** XRD characterization of doped hematite above 8% with Ni and Zn, showing the appearance of additional crystalline phases . Asterisks correspond with the pattern of α-Fe$_2$O$_3$ hexagonal hematite (ICSD code 15840) and red squares correspond to the appearance of a second spinel phase (ICSD 52387). Red stands for iron oxides and Ni and Zn are represented in orange and green, respectively.

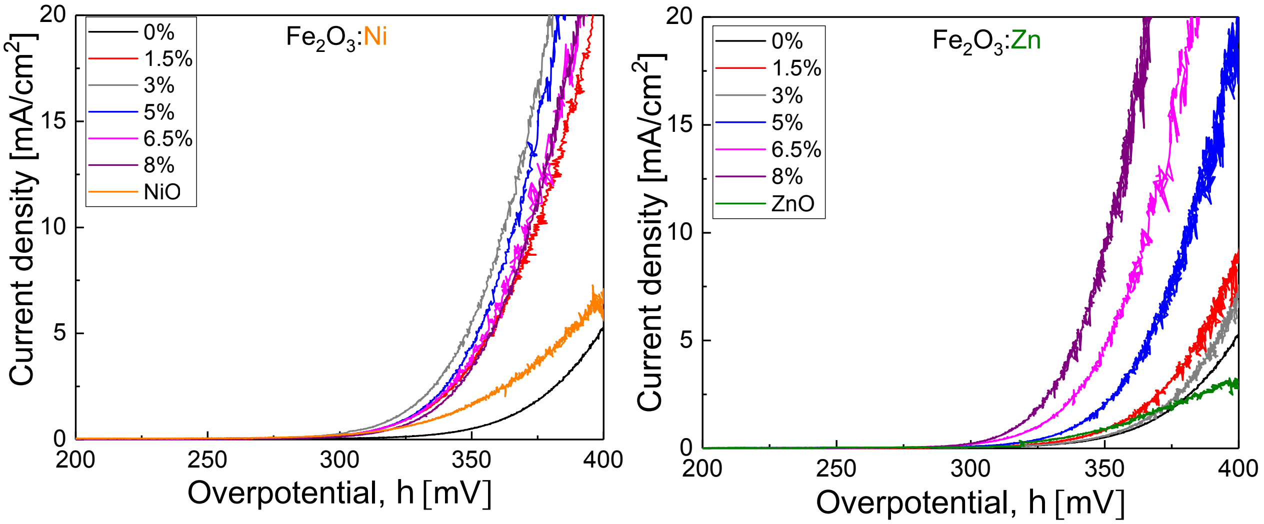

Figure S2 a) LSVs for hematite doped with Ni. The orange line corresponds to NiO synthetized and measured with the same protocol. (b) LSVs for hematite doped with Zn, the green line corresponds to ZnO activity in basic media, as we mention before, this sample was obtained using the same procedures as the doped-hematite.

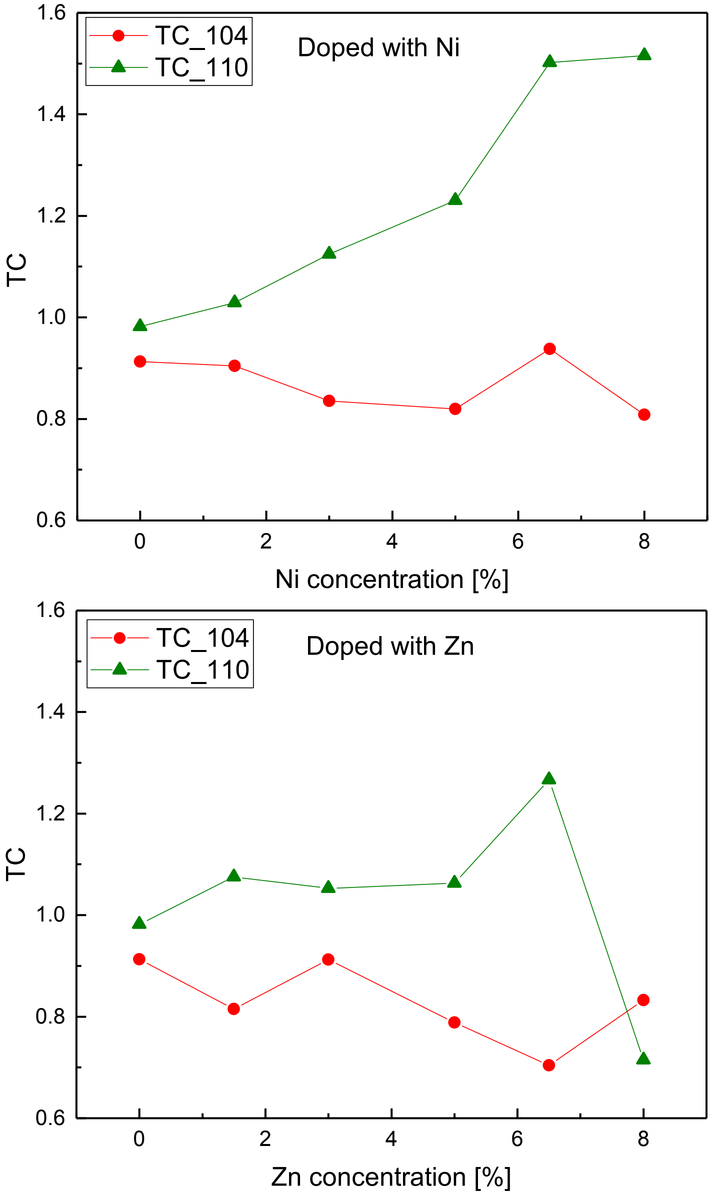

Figure S3 Comparison of the texture coefficient for the hematite reflections (110) and (104) upon Ni (top) or Zn (bottom) doping.

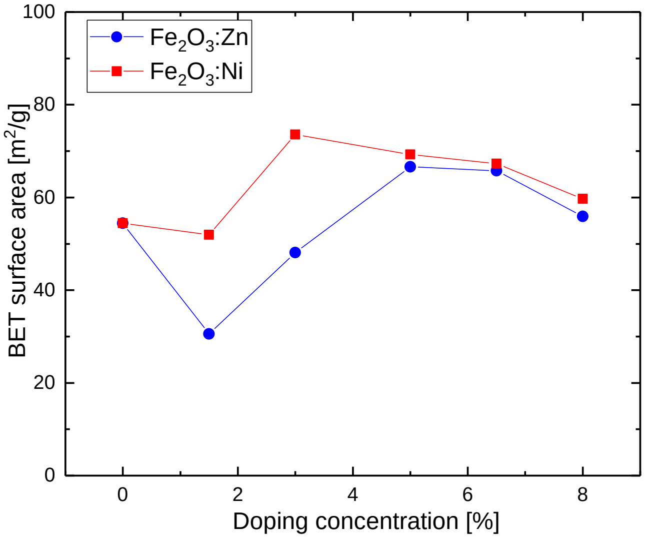

Figure S4 BET surface area vs doping concentration for both dopants.

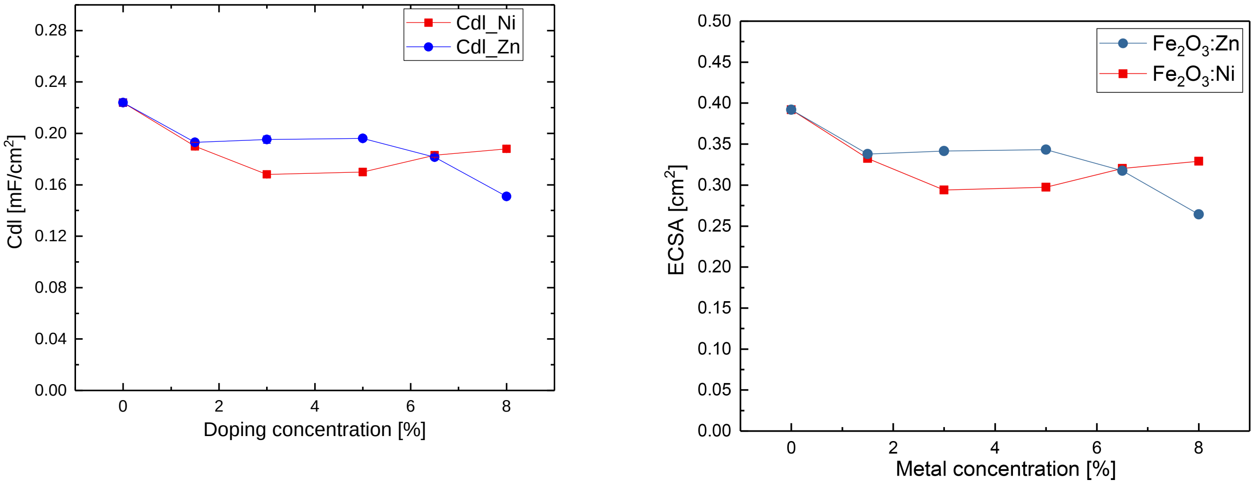

Figure S5 Double layer capacitance, and the corresponding electrochemical surface area(ECSA), vs doping concentration for both dopants.

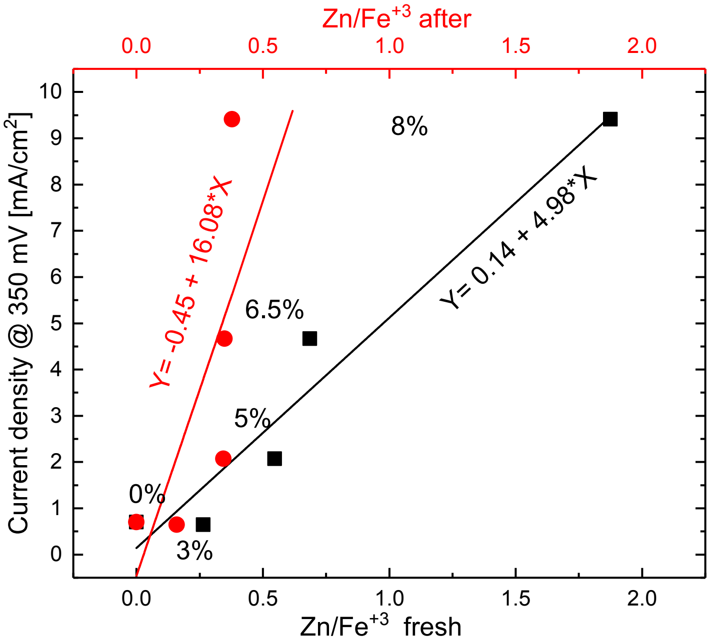

Figure S6 Current density at η = 350 mV overpotential as a function of Zn^{+2}/Fe^{+3} ratio found before (black squares) and after (red circles) two hours electrolysis (red points). The Zn:Fe ratio decreases during water oxidation, as observed in ICP data.

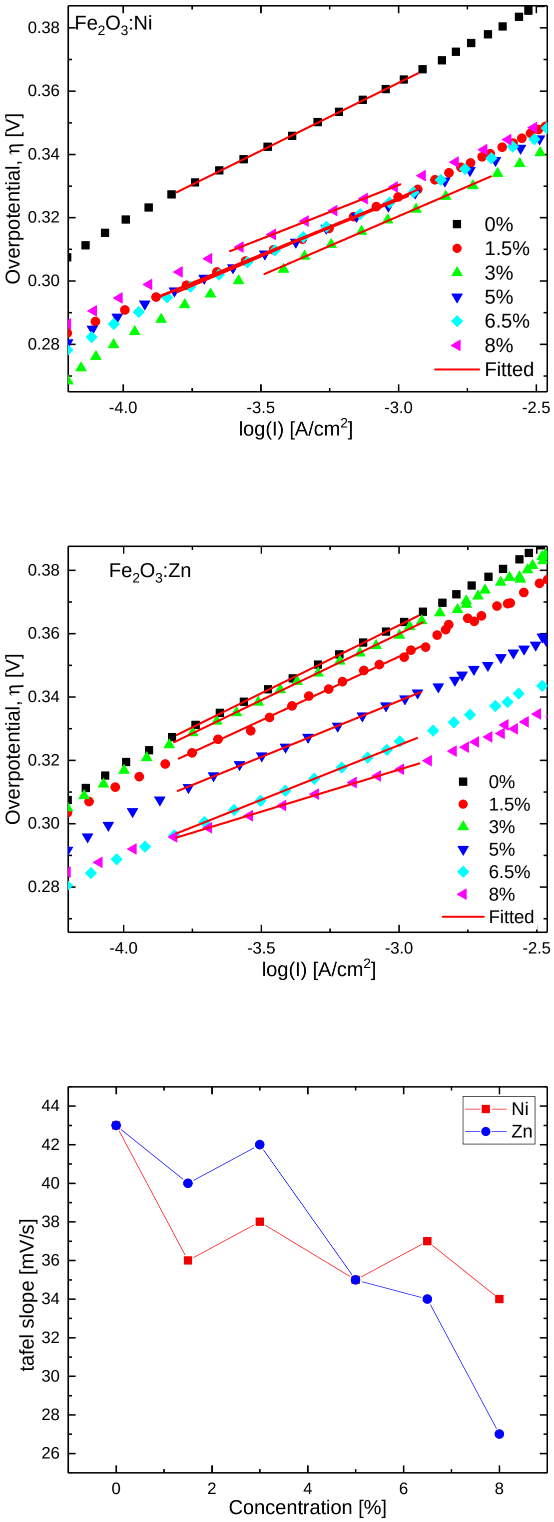

Figure S7 Tafel analysis of the LSV data for Ni:Fe_2O_3 (top), Zn:Fe_2O_3 (middle) and summary of Tafel slope vs doping (bottom).

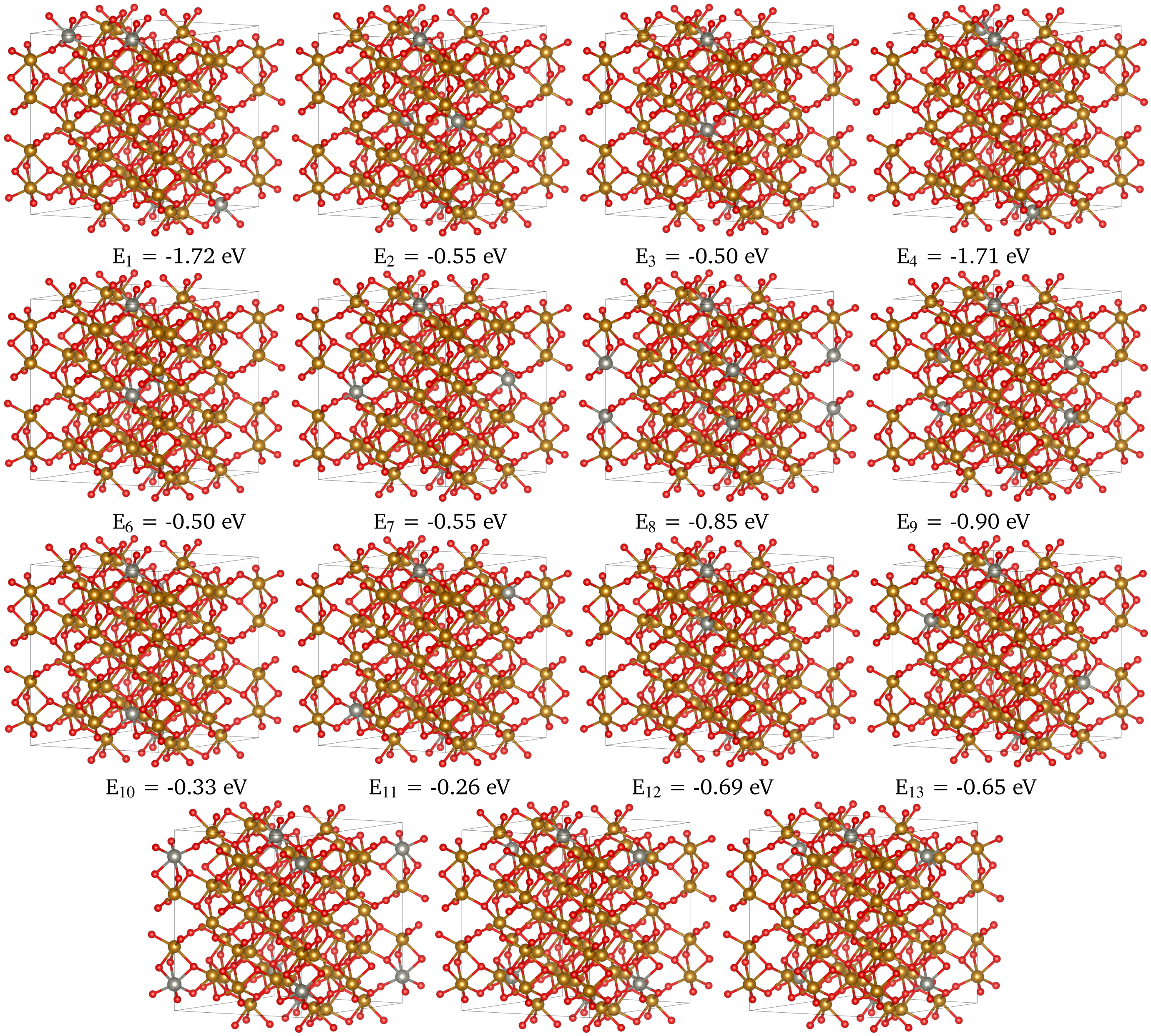

E_1 = -1.72 eV
E_2 = -0.55 eV
E_3 = -0.50 eV
E_4 = -1.71 eV

E_6 = -0.50 eV
E_7 = -0.55 eV
E_8 = -0.85 eV
E_9 = -0.90 eV

E_{10} = -0.33 eV
E_{11} = -0.26 eV
E_{12} = -0.69 eV
E_{13} = -0.65 eV

E_{14} = -0.00 eV
E_{15} = -0.07 eV
E_{17} = -0.07 eV

Figure S8 List of non-equivalent configurations for the 2x2x1 supercell of hematite for four replacements of Fe by Zn. Energy is the difference with the highest energy configuration (0 eV is the highest i.e. the most unstable).

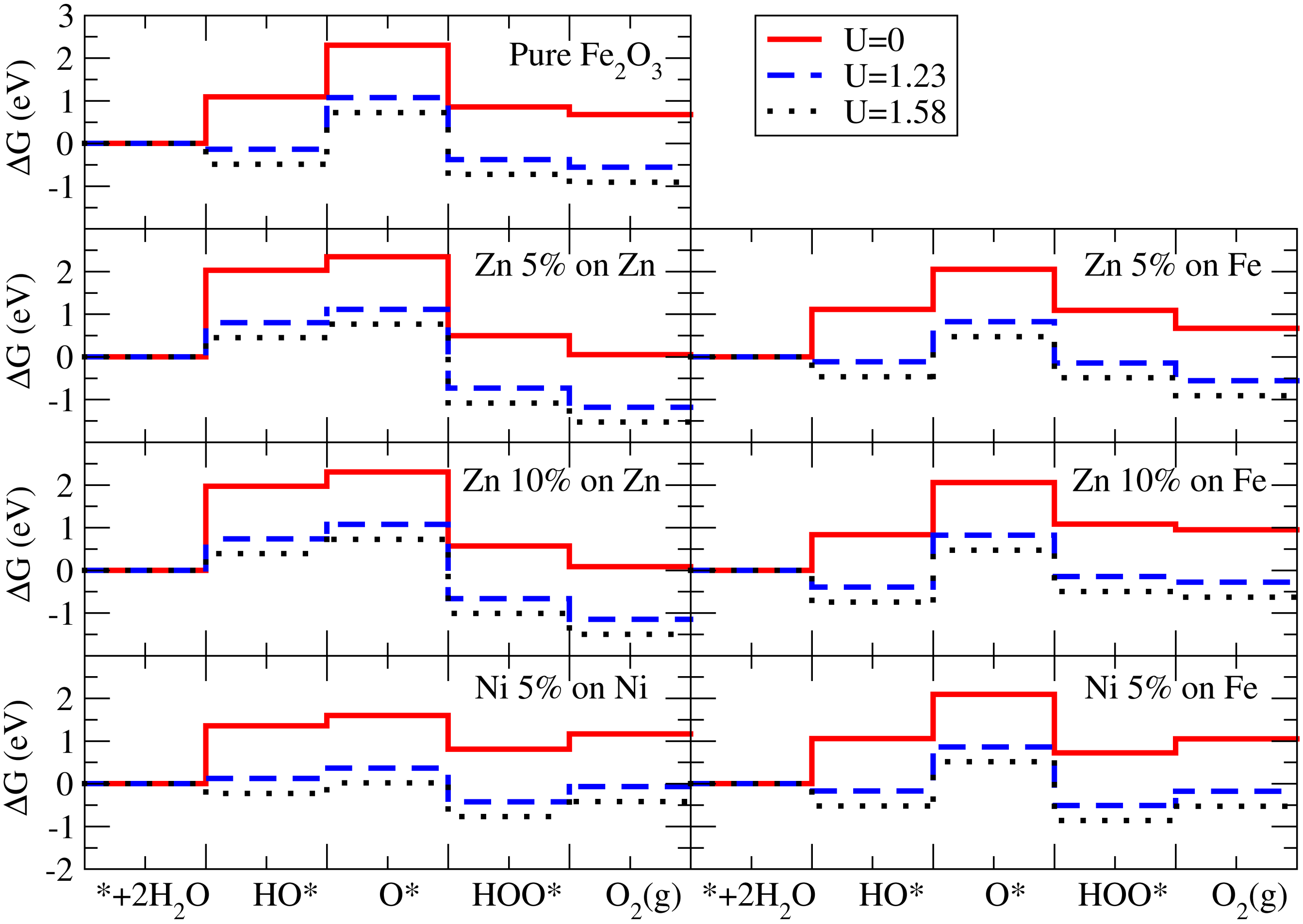

Figure S9 Gibbs' free energy diagrams for the OER reaction on each of the potential active sites.

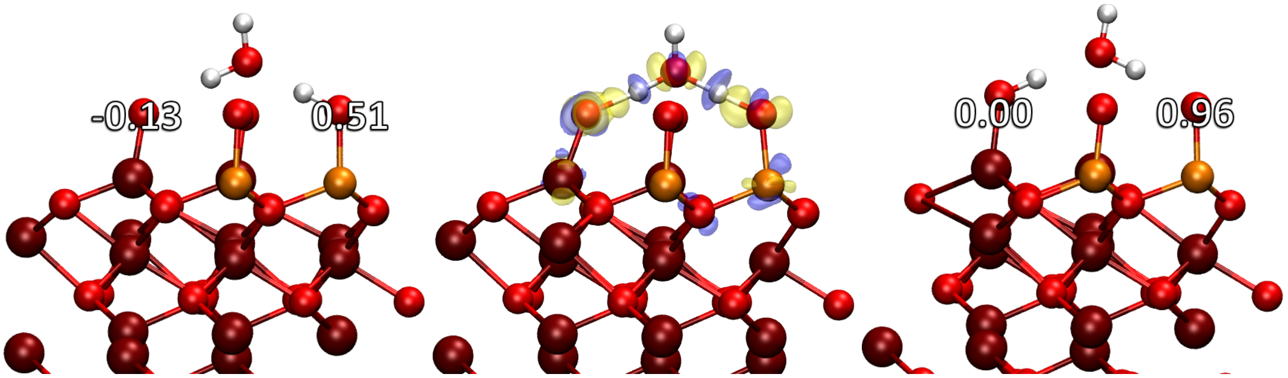

Figure S10 Initial, transition and final stated for the H transfer between Ni and Fe centers in Ni:Fe$_2$O$_3$. For the transition state the different density with respect to H$_3$O and the surface is presented: blue density corresponds to negative difference, and yellow to positive. The numbers in the atoms are their magnetization in μ_B.

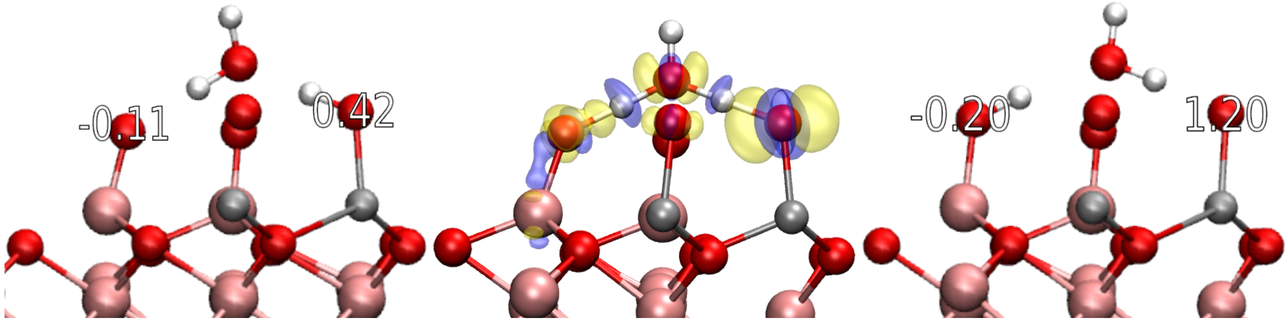

Figure S11 Initial, transition and final stated for the H transfer between Ni and Fe centers in Zn:Fe_2O_3. For the transition state the different density with respect to H_3O and the surface is presented: blue density corresponds to negative difference, and yellow to positive. The numbers in the atoms are their magnetization in μ_B.

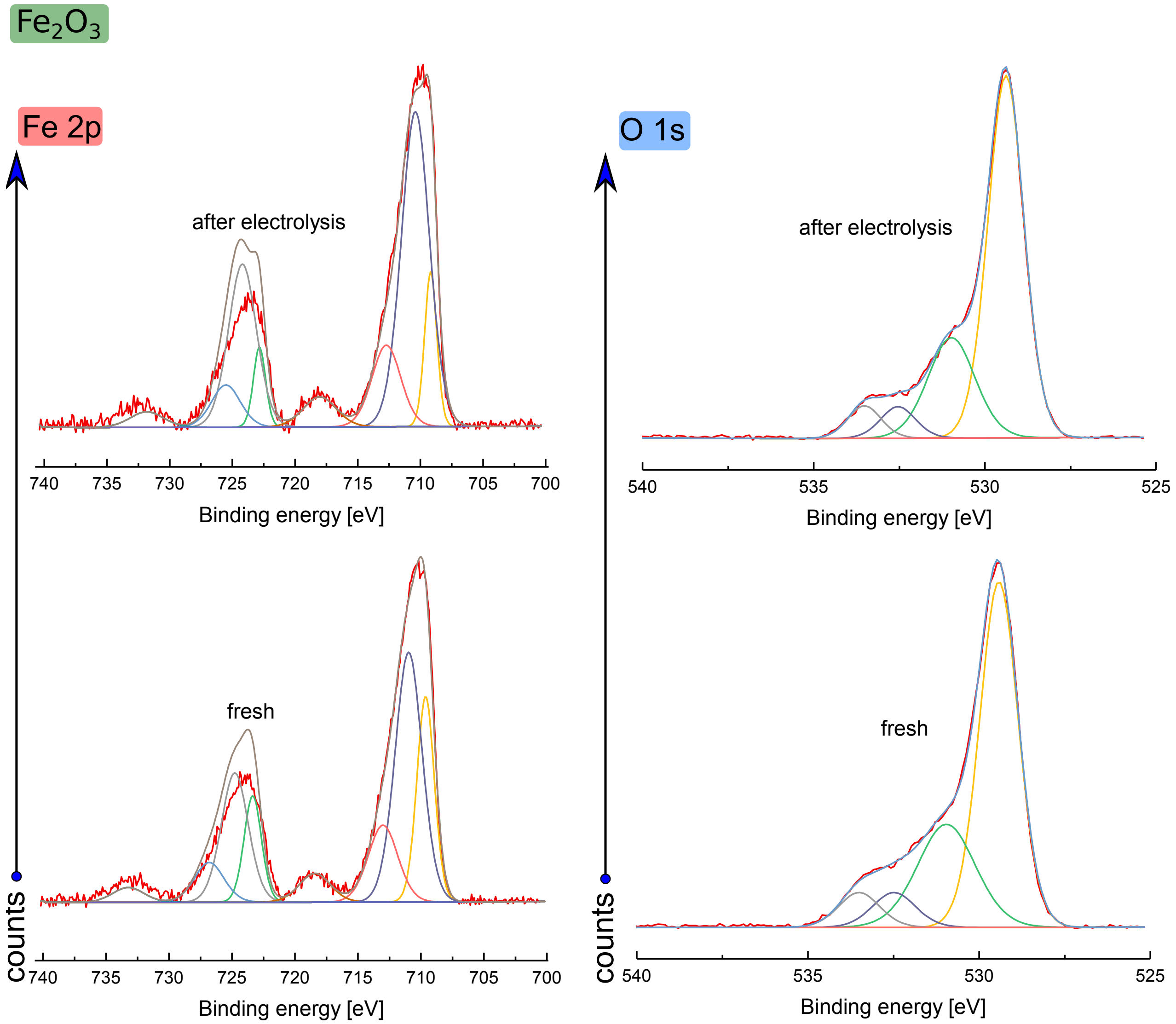

Figure S12 XPS data (Fe and O edges) for Fe_2O_3 before and after 2 h electrocatalytic water oxidation at a constant current density of 10 mA/cm^2 in 0.1 M KOH (pH 13).

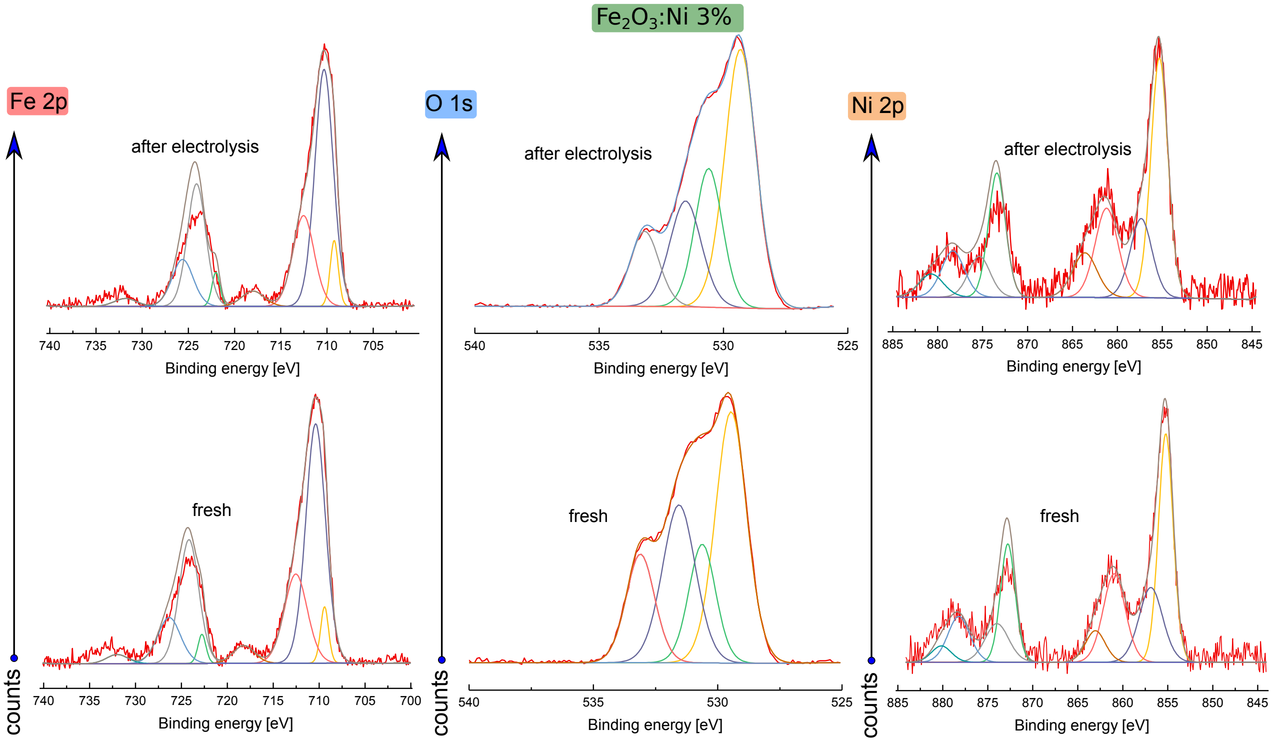

Figure S13 XPS data (Ni, Fe and O edges) for Fe_2O_3 doped with Ni at 3% before and after 2 h electrocatalytic water oxidation at a constant current density of 10 mA/cm^2 in 0.1 M KOH (pH 13).

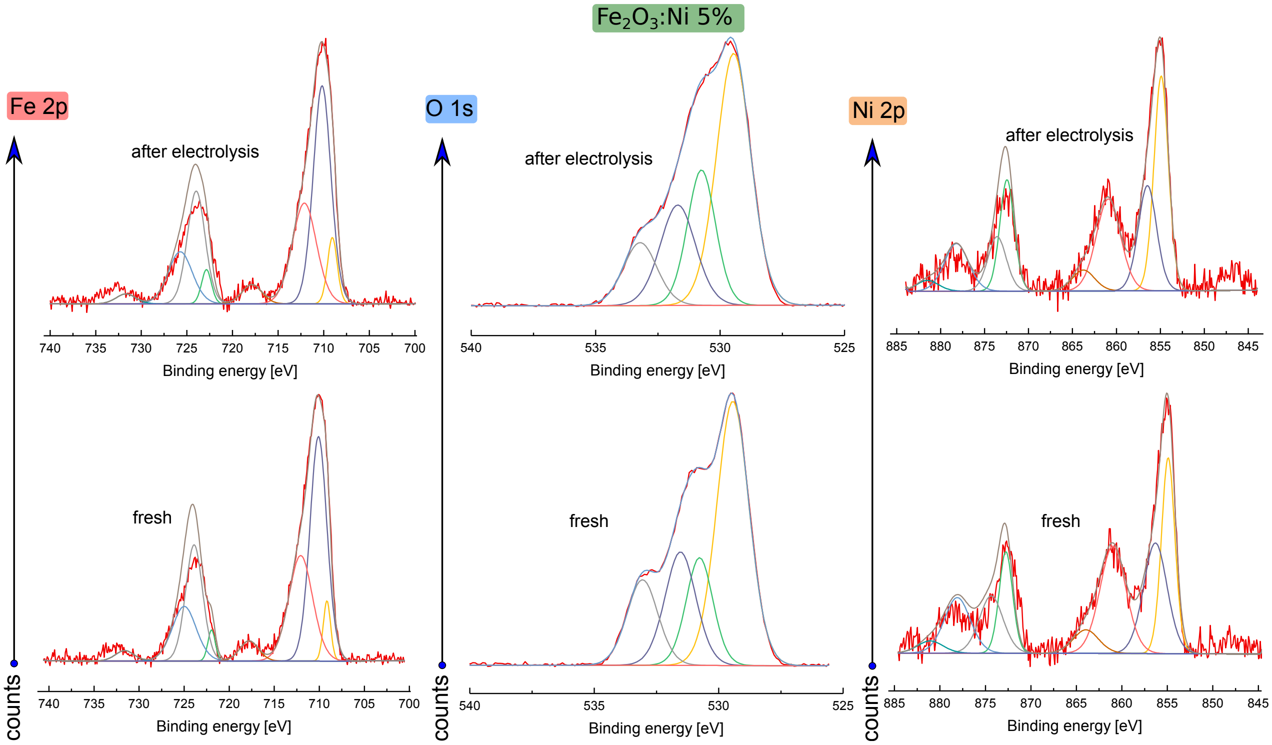

Figure S14 XPS data (Ni, Fe and O edges) for Fe_2O_3 doped with Ni at 5% before and after 2 h electrocatalytic water oxidation at a constant current density of 10 mA/cm^2 in 0.1 M KOH (pH 13).

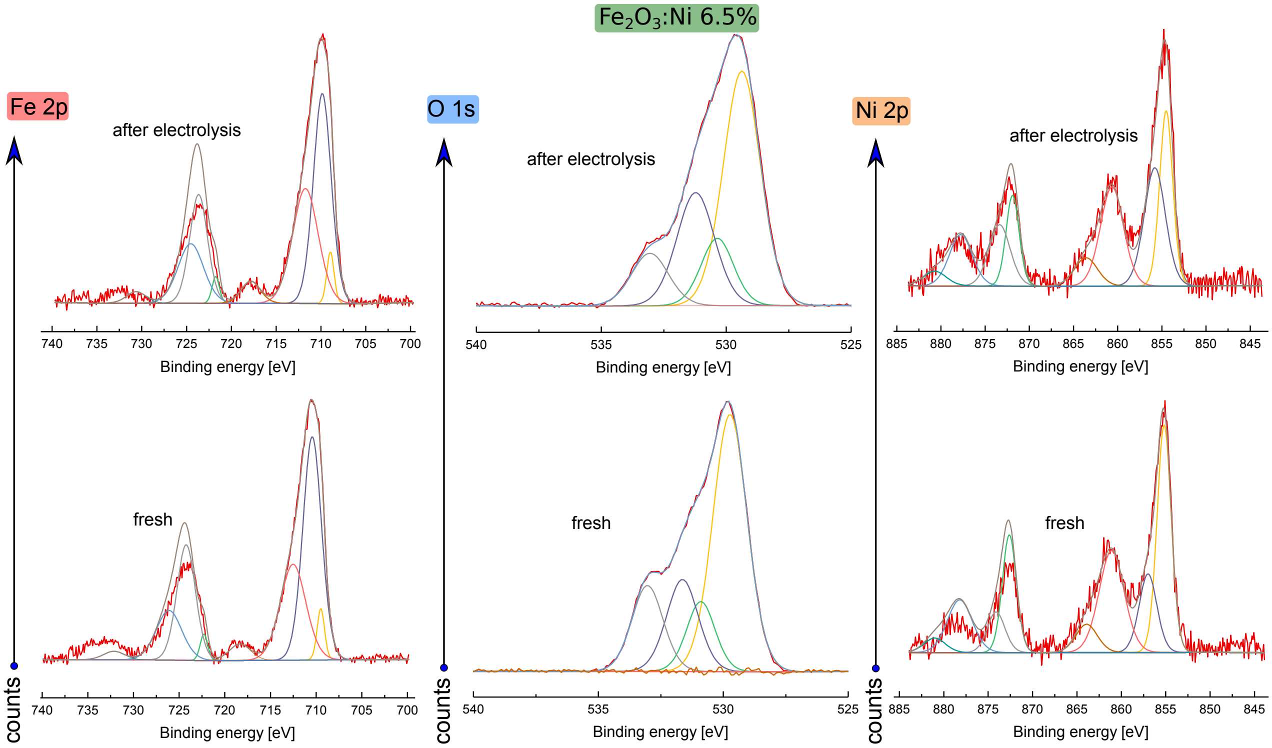

Figure S15 XPS data (Ni, Fe and O edges) for Fe_2O_3 doped with Ni at 6.5% before and after 2 h electrocatalytic water oxidation at a constant current density of 10 mA/cm^2 in 0.1 M KOH (pH 13).

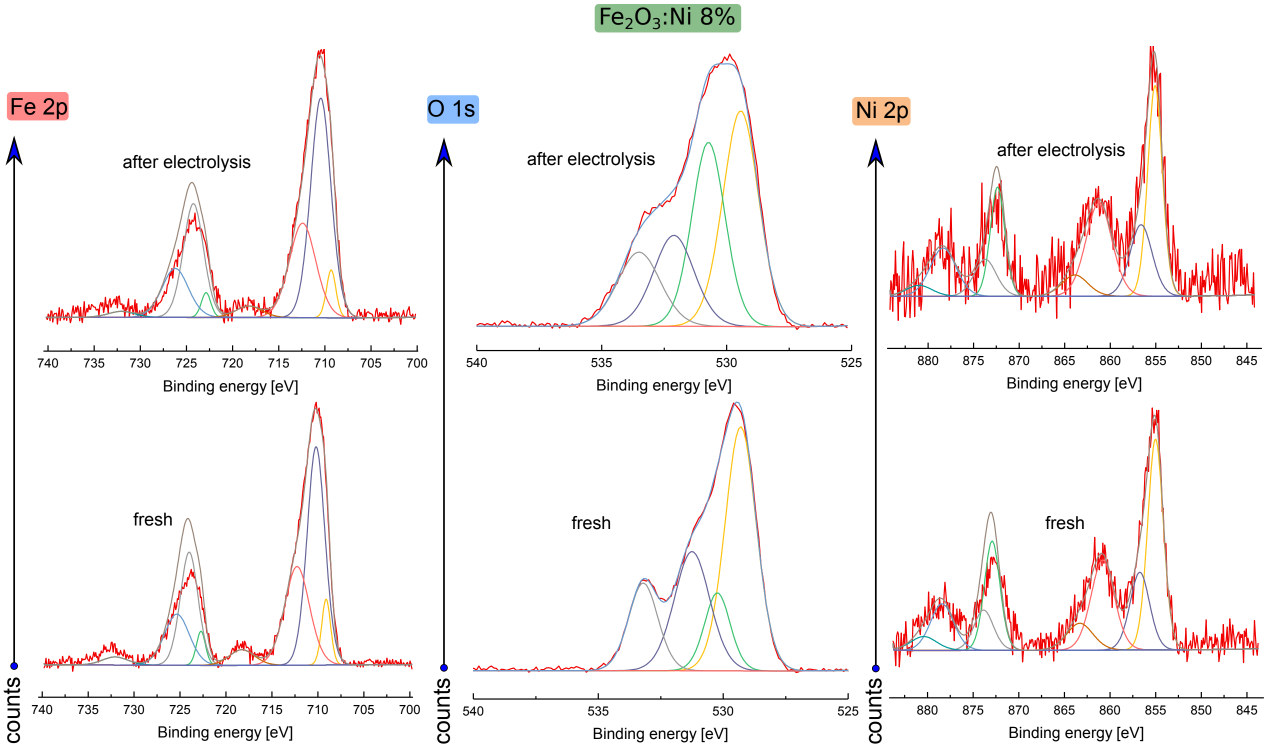

Figure S16 XPS data (Ni, Fe and O edges) for Fe_2O_3 doped with Ni at 8% before and after 2 h electrocatalytic water oxidation at a constant current density of 10 mA/cm^2 in 0.1 M KOH (pH 13).

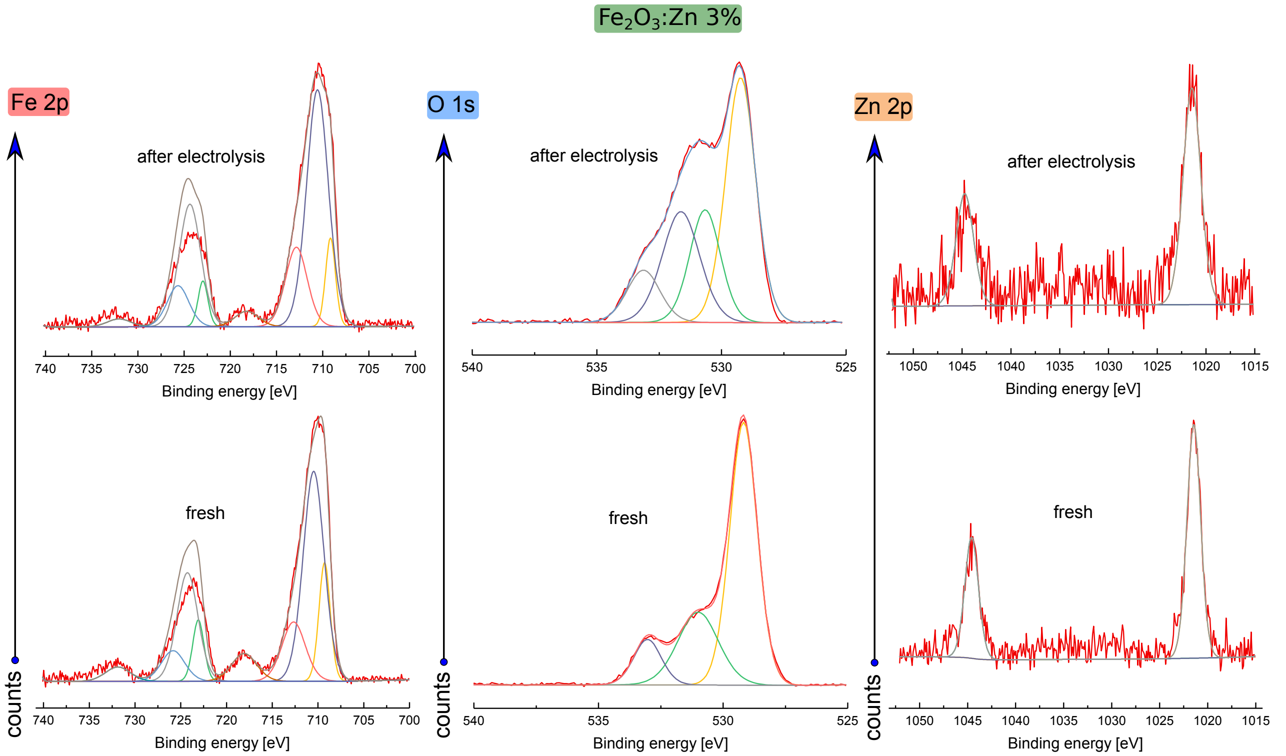

Figure S17 XPS data (Zn, Fe and O edges) for Fe_2O_3 doped with Zn at 3% before and after 2 h electrocatalytic water oxidation at a constant current density of 10 mA/cm^2 in 0.1 M KOH (pH 13).

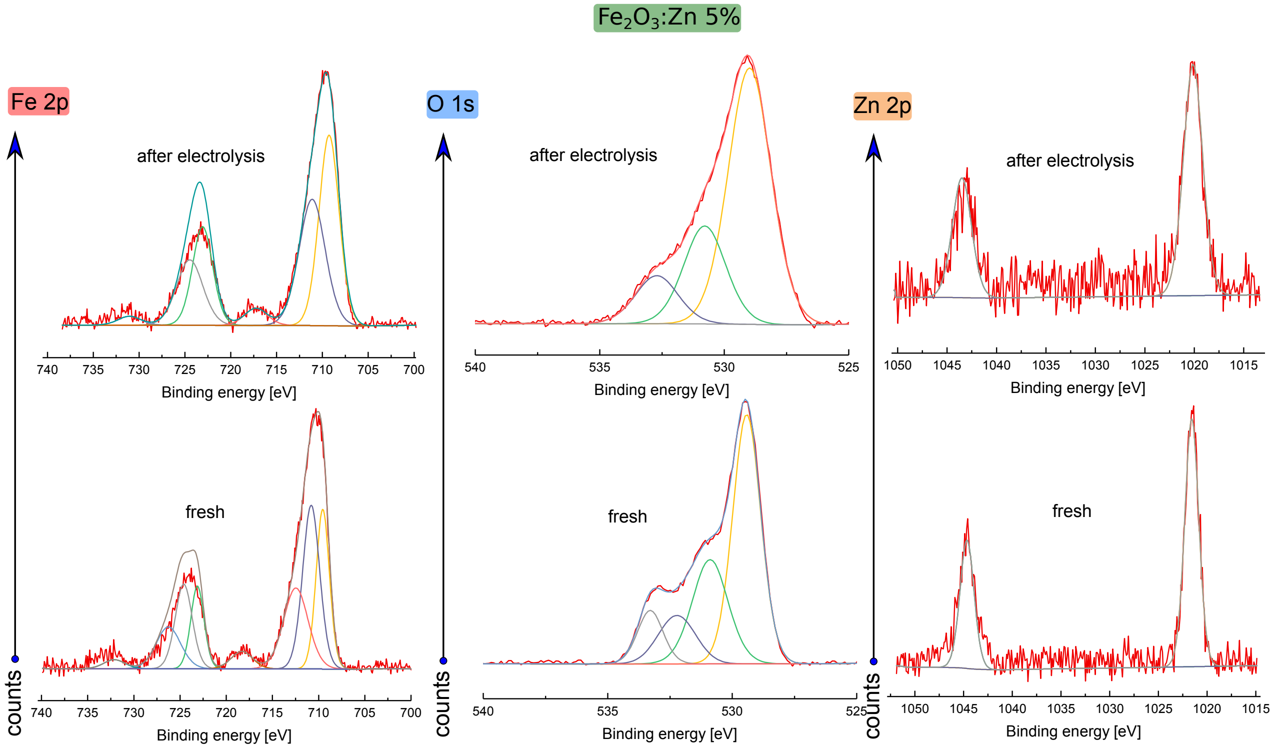

Figure S18 XPS data (Zn, Fe and O edges) for Fe_2O_3 doped with Zn at 5% before and after 2 h electrocatalytic water oxi dation at a constant current density of 10 mA/cm^2 in 0.1 M KOH (pH 13).

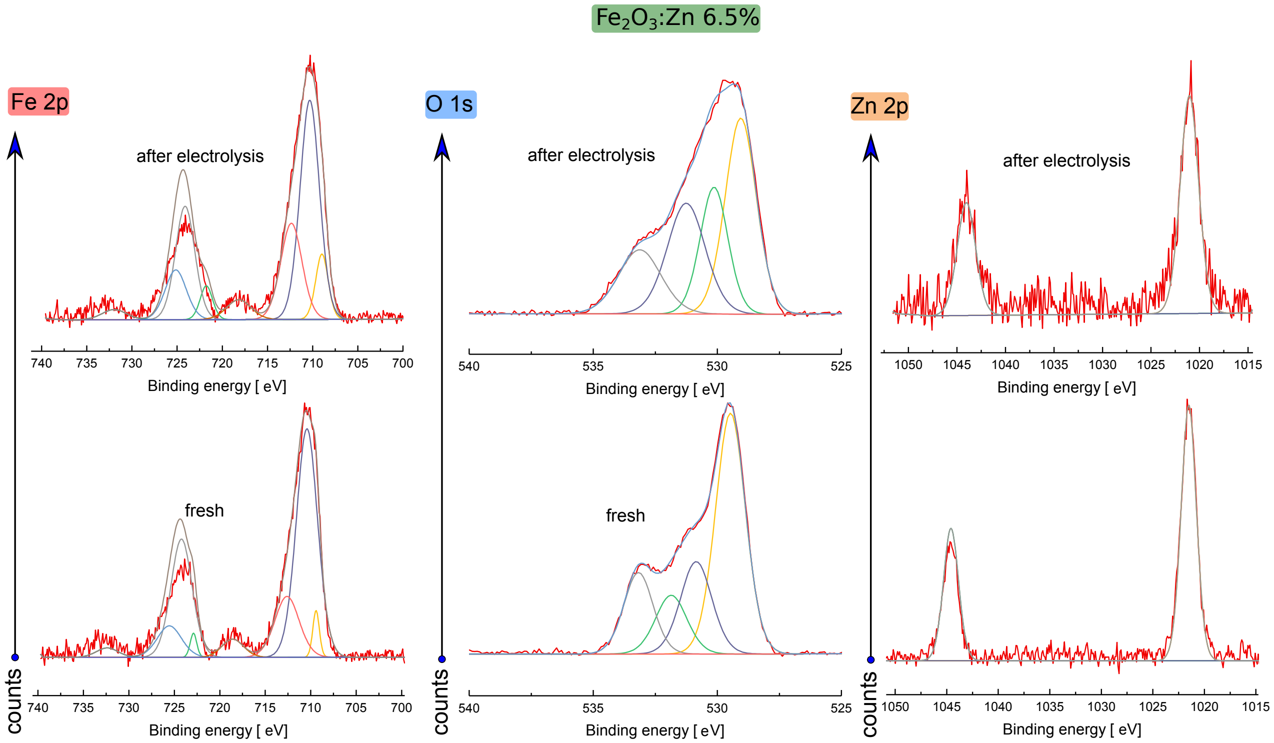

Figure S19 XPS data (Zn, Fe and O edges) for Fe_2O_3 doped with Zn at 6.5% before and after 2 h electrocatalytic water oxidation at a constant current density of 10 mA/cm^2 in 0.1 M KOH (pH 13).

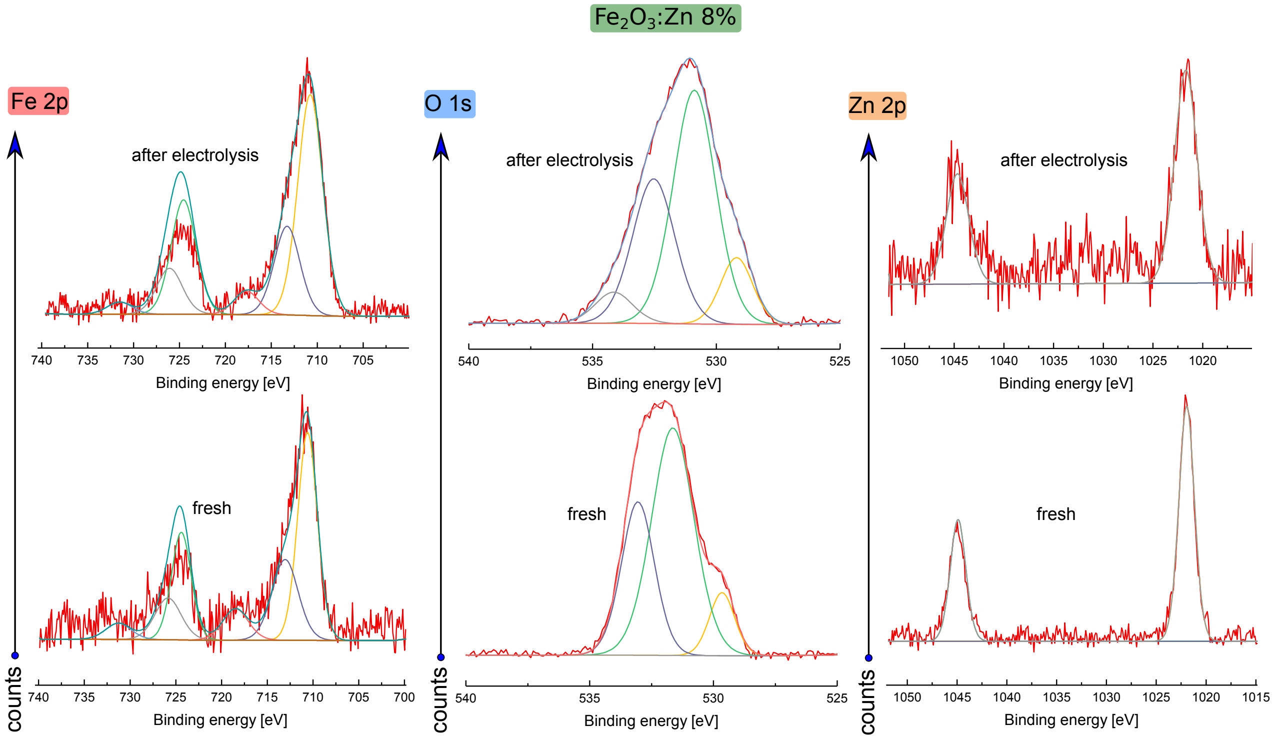

Figure S20 XPS data (Zn, Fe and O edges) for Fe_2O_3 doped with Zn at 8% before and after 2 h electrocatalytic water oxidation at a constant current density of 10 mA/cm^2 in 0.1 M KOH (pH 13).

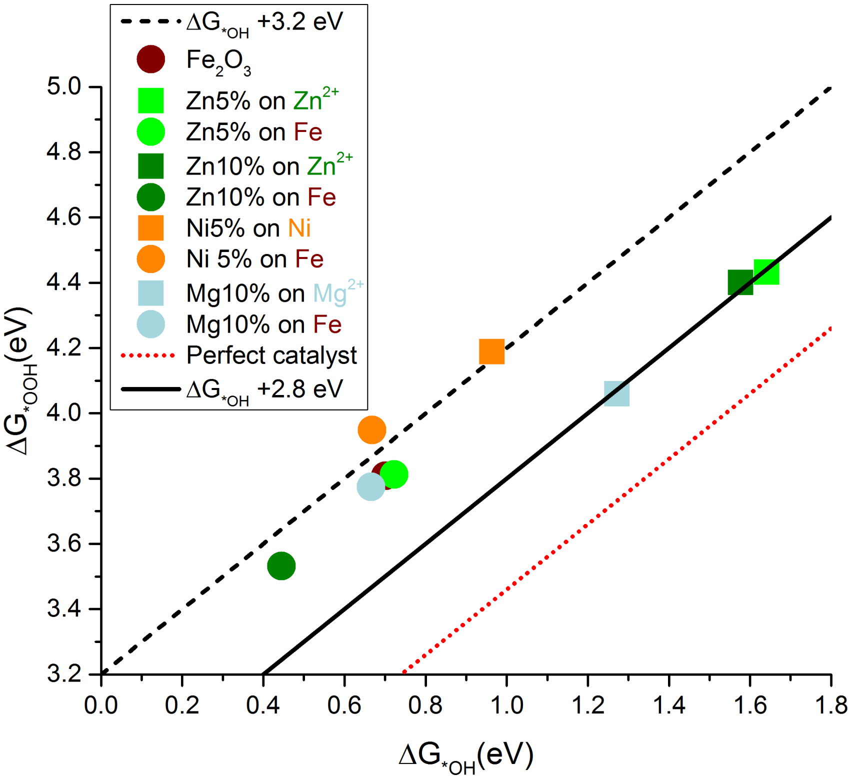

Figure S21 Scaling relation between $\Delta G_{*\text{OOH}}$ and $\Delta G_{*\text{OH}}$ without ZPE-TS correction. The highest dotted line corresponds to the redox dopants and shows an offset +3.2 eV. The solid line correspond to an offset of +2.8 eV and corresponds to the non-redox dopants. The lower red dashed line corresponds to the ideal theoretical catalyst with an offset of +2.46. All lines have slope 1.

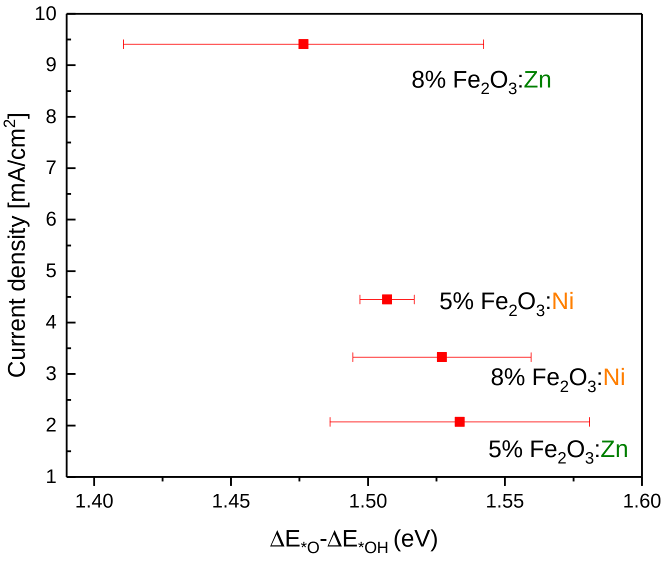

Figure S22 Binding energy estimates: the current taken at 350 mV overpotential provides the experimental ΔG_{*O}-ΔG_{*OH} according to the procedure described in the Binding energy Measurements section.

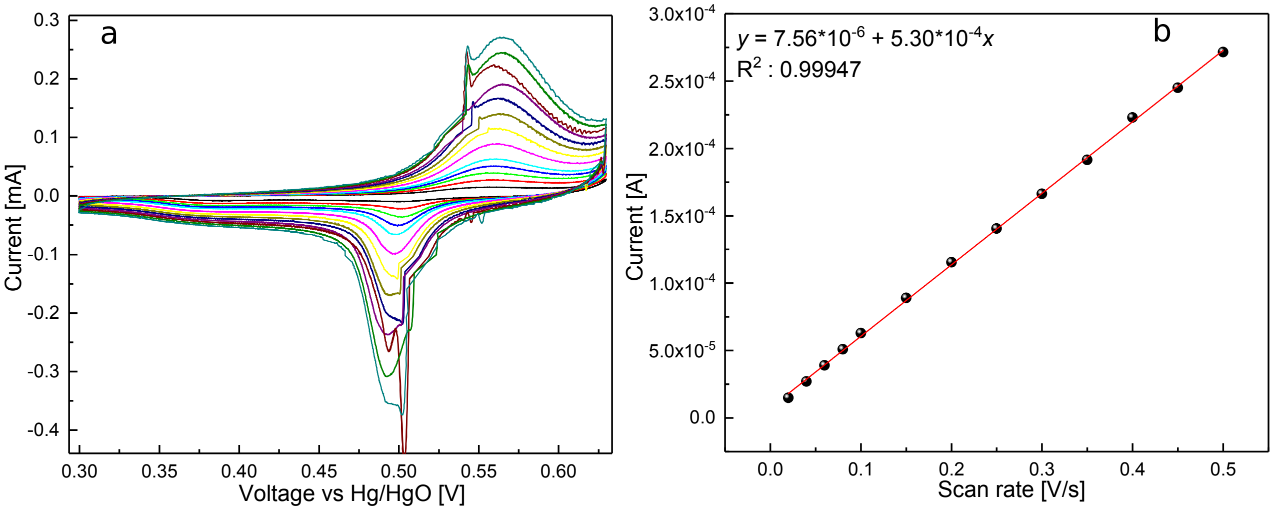

Figure S23 a) Pre-catalytic region of the cyclic voltammograms of Zn:Fe_2O_3 (8%) in 0.1 M KOH (pH 13) at different scan rates. b) Linear dependence of the peak current of the Co3+/Co2+ reduction wave vs scan rate. The concentration of redox active centres was calculated from the slope as described in the TOF estimation section.

Metal concentration (%)	Zn leaching (%)	Ni leaching (%)	Fe leaching (%)
0.0	*	*	< 0.001
3.0	0.045	< 0.021	< 0.001
5.0	0.022	< 0.013	< 0.001
6.5	0.033	< 0.010	< 0.001
8.0	0.022	< 0.009	< 0.001

Table S1 ICP-OES analysis of the liquid reaction media after 2 h of electrocatalytic water oxidation at a constant current density of 10 mA/cm^2 in KOH (0.1 M) for both families of doped-oxides.

	DFT+U	Experiment	Ref[16]	Ref Exp
a(Å)	5.11	5.033 ±0.006	5.12	5.035[17]
c(Å)	13.96	13.77±0.024	13.94	13.747[17]
Polarization (Fe)(μ_B)	4.04	3.6	4.29	4.9[18]
Bandgap (eV)	1.81	2.04	2	[2.0,2.2][19]

Table S2 Bulk results comparison between DFT and experiments

	ZPE (eV)	TS (eV)	ZPE-TS (eV)
H_2O	0.580	0.67	-0.09
H_2	0.327	0.41	-0.07
O_2	0.097	0.64	-0.54
*OH	0.371	0.03	0.34
*OOH	0.442	0.06	0.38
*O	0.073	0.02	0.05

Table S3 Zero point vibrational energy and entropic contribution to the free energy at the standard condition for the hematite (pH 0, P = 1 bar, T = 298 K) as obtained from published data.[20]

Composition	ΔG_1(eV)	ΔG_2(eV)	ΔG_3(eV)	ΔG_4(eV)	G^{OER}(eV)
Fe_2O_3 (100%)	1.091	2.302	0.853	0.674	2.302
Zn:Fe_2O_3 (2:48) on Zn	2.031	2.344	0.495	0.050	2.344
Zn:Fe_2O_3 (2:48) on Fe	1.112	2.051	1.087	0.670	2.051
Zn:Fe_2O_3 (4:48) on Zn	1.967	2.304	0.568	0.082	2.304
Zn:Fe_2O_3 (4:48) on Fe	0.835	2.053	1.081	0.951	2.053
Ni:Fe_2O_3 (2:48) on Ni	1.353	1.597	0.807	1.163	1.597
Ni:Fe_2O_3 (2:48) on Fe	1.058	2.092	0.719	1.051	2.092
Mg:Fe_2O_3 (4:48) on Mg	1.661	2.430	0.405	0.424	2.430
Mg:Fe_2O_3 (4:48) on Fe	1.056	1.936	1.220	0.708	1.936

Table S4 Free energy for the WNA path on a single site at 298.15 K, p = 0.035 bar, pH 0, U = 0 V.

Composition	ΔG_1(eV)	ΔG_2(eV)	ΔG_3(eV)	ΔG_4(eV)	G^{OER}(eV)
Fe_2O_3 (100%)	-0.139	1.072	-0.377	-0.556	1.072
Zn:Fe_2O_3 (2:48) on Zn	0.801	1.114	-0.735	-1.180	1.114
Zn:Fe_2O_3 (2:48) on Fe	-0.118	0.821	-0.143	-0.560	0.821
Zn:Fe_2O_3 (4:48) on Zn	0.737	1.074	-0.662	-1.148	1.074
Zn:Fe_2O_3 (4:48) on Fe	-0.395	0.823	-0.149	-0.279	0.823
Ni:Fe_2O_3 (2:48) on Ni	0.123	0.367	-0.423	-0.067	0.367
Ni:Fe_2O_3 (2:48) on Fe	-0.172	0.862	-0.511	-0.179	0.862
Mg:Fe_2O_3 (4:48) on Mg	0.431	1.200	-0.825	-0.806	1.200
Mg:Fe_2O_3 (4:48) on Fe	-0.174	0.706	-0.010	-0.522	0.706

Table S5 Free energy for the WNA path on a single site at 298.15 K, p = 0.035 bar, pH 0, U = 1.23 V.

Composition	ΔG_1(eV)	ΔG_2(eV)	ΔG_3(eV)	ΔG_4(eV)	G^{OER}(eV)
Fe_2O_3 (100%)	-0.489	0.722	-0.727	-0.906	0.722
Zn:Fe_2O_3 (2:48) on Zn	0.451	0.764	-1.085	-1.530	0.764
Zn:Fe_2O_3 (2:48) on Fe	-0.468	0.471	-0.493	-0.910	0.471
Zn:Fe_2O_3 (4:48) on Zn	0.387	0.724	-1.012	-1.498	0.724
Zn:Fe_2O_3 (4:48) on Fe	-0.745	0.473	-0.499	-0.629	0.473
Ni:Fe_2O_3 (2:48) on Ni	-0.227	0.017	-0.773	-0.417	0.017
Ni:Fe_2O_3 (2:48) on Fe	-0.522	0.512	-0.861	-0.529	0.512
Mg:Fe_2O_3 (4:48) on Mg	0.081	0.850	-1.175	-1.156	0.850
Mg:Fe_2O_3 (4:48) on Fe	-0.524	0.356	-0.360	-0.872	0.356

Table S6 Free energy for the WNA path on a single site at 298.15 K, p = 0.035 bar, pH 0, U = 1.58 V.

	Energy difference with top layer(eV)
Ni11	0
Ni12	-0.271
Ni13	0.789
Ni14	1.181
Ni15	0.904

Table S7 Energy difference for the second Ni atom substituting an Fe site in the lattice. The lowest energy configuration for doping with one Ni atom is on the top. The position of the second Ni atom is not necessarily on the top. The results shows that the second Ni prefer to sit on the second layer (first layer being the top).

Composition	G_{*OOH}	G_{*OH}	G_{*O}
Fe_2O_3 (100%)	3.81	0.70	3.33
Zn:Fe_2O_3 (2:48) on Zn	4.43	1.64	4.31
Zn:Fe_2O_3 (2:48) on Fe	3.81	0.72	3.10
Zn:Fe_2O_3 (4:48) on Zn	4.40	1.58	3.95
Zn:Fe_2O_3 (4:48) on Fe	3.53	0.45	2.83
Ni:Fe_2O_3 (2:48) on Ni	4.19	0.96	2.89
Ni:Fe_2O_3 (2:48) on Fe	3.95	0.67	3.09
Mg:Fe_2O_3 (4:48) on Mg	4.06	1.27	4.03
Mg:Fe_2O_3 (4:48) on Fe	3.77	0.67	2.93

Table S8 DFT-calculated binding energies in eV without ZPE correction

Catalyst	Current density at 1.57V vs RHE mA/cm^2	TOF s^{-1}	pH; concentration	ref
Fe_2O_3/Zn-Co-LDH	1.700	-	14.0; 1M KOH	[21]
Fe_2O_3/Zn$(OH)_2$	0.040	-	14.0; 1M KOH	[21]
Fe_2O_3/Co-$(OH)_2$	0.380	-	14.0; 1M KOH	[21]
Fe_2O_3	0.001	-	14.0; 1M KOH	[21]
Fe_2O_3	0.250	-	13.6; 1M NaOH	[22]
H-Fe_2O_3	0.033	-	13.6; 1M NaOH	[22]
$NiFeO_xH_y$	4.130	∼1.000	14.0; 1M KOH	[23]*
LDH FeCo	1.640	0.009	14.0; 1M KOH	[24]
A-FeCoW	1.870	0.170	14.0; 1M KOH	[24]
G-FeCo	1.640	0.46	14.0; 1M KOH	[24]
Fe_2O_3:Sn 400ijC	0.400	-	13.6; 1M NaOH	[25]
Sn:Fe_2O_3:Sn 800ijC	0.100	-	13.6; 1M NaOH	[25]
Fe_2O_3:Pt	0.200	-	13.6; 1M NaOH	[26]
Fe_2O_3:W	0.180	-	13.8; 1M NaOH	[27]
Fe_2O_3:Mo	0.200	-	13.8; 1M NaOH	[27]
NiFe LDH	0.200	-	13.6; 1M NaOH	[28]
Fe_2O_3:Pt	0.200	-	13.6; 1M NaOH	[28]
Fe_2O_3:Zn 8%	9.501	0.277	13.0; 0.1M KOH	this work
Fe_2O_3:Ni 3%	5.612	0.120	13.0; 0.1M KOH	this work

Table S9 Comparison of OER electrocatalytic activity of 2D electrodes in basic media. (*) is no considering the area electrode

References

[1] S. Pintado, S. Goberna-Ferron, E. C. Escudero-Adan and J. R. Galan-Mascaros, *J. Am. Chem. Soc*, 2013, **135**, 13270–13273.

[2] D.-Y. Kuo, J. K. Kawasaki, J. N. Nelson, J. Kloppenburg, G. Hautier, K. M. Shen, D. G. Schlom and J. Suntivich, *J. Am. Chem. Soc.*, 2017, **139**, 3473–3479.

[3] R. Grau-Crespo, S. Hamad, C. R. A. Catlow and N. H. De Leeuw, *J. Phys. Condens. Matter*, 2007, **19**, 256201.

[4] G. Kresse and D. Joubert, *Phys. Rev. B*, 1999, **59**, 1758–1775.

[5] J. Rossmeisl, Z.-W. Qu, H. Zhu, G.-J. Kroes and J. Nørskov, *J. Electroanal. Chem.*, 2007, **607**, 83–89.

[6] J. K. Nørskov, J. Rossmeisl, A. Logadottir, L. Lindqvist, J. R. Kitchin, T. Bligaard and H. Jónsson, *J. Phys. Chem. B*, 2004, **108**, 17886–17892.

[7] A. Valdés, Z.-W. Qu, G.-J. Kroes, J. Rossmeisl and J. K. Nørskov, *J. Phys. Chem. C*, 2008, **112**, 9872–9879.

[8] A. Valdés and G.-J. Kroes, *J. Chem. Phys.*, 2009, **130**, 114701.

[9] A. Hellman and R. G. S. Pala, *J. Phys. Chem.C*, 2011, **115**, 12901–12907.

[10] P. Liao, J. A. Keith and E. A. Carter, *J. Am. Chem. Soc*, 2012, **134**, 13296–13309.

[11] M.-T. Nguyen, N. Seriani, S. Piccinin and R. Gebauer, *J. Chem. Phys.*, 2014, **140**, 064703.

[12] J. Rossmeisl, A. Logadottir and J. Nørskov, *Chem. Phys.*, 2005, **319**, 178–184.

[13] A. J. Bard and M. A. Fox, *Acc. Chem. Res*, 1995, **28**, 141–145.

[14] I. C. Man, H.-Y. Su, F. Calle-Vallejo, H. A. Hansen, J. I. Martínez, N. G. Inoglu, J. Kitchin, T. F. Jaramillo, J. K. Nørskov and J. Rossmeisl, *ChemCatChem*, 2011, **3**, 1159–1165.

[15] A. Einstein, *Ann. Phys.*, 1905, **17**, 549–560.

[16] M.-t. Nguyen, N. Seriani and R. Gebauer, *J. Chem. Phys.*, 2013, **138**, 194709.

[17] L. W. Finger and R. M. Hazen, *J. Appl. Phys.*, 1980, **51**, 5362–5367.

[18] E. Krén, P. Szabó and G. Konczos, *Phys. Lett.*, 1965, **19**, 103–104.

[19] J. Lee and S. Han, *Phys. Chem. Chem. Phys.*, 2013, **15**, 18906.

[20] A. Hellman and R. G. S. Pala, *J. Phys. Chem.C*, 2011, **115**, 12901–12907.

[21] D. Xu, Y. Rui, Y. Li, Q. Zhang and H. Wang, *Appl. Surf. Sci.*, 2015, **358**, 436–442.

[22] Y. Yin, X. Zhang, L. Li, L. Spiccia and C. Sun, *J. Phys. Chem. C*, 2017, **121**, 16059–16065.

[23] C. Roy, B. Sebok, S. B. Scott, E. M. Fiordaliso, J. E. Sørensen, A. Bodin, D. B. Trimarco, C. D. Damsgaard, P. C. K. Vesborg, O. Hansen, I. E. L. Stephens, J. Kibsgaard and I. Chorkendorff, *Nat. Catal.*, 2018, **1**, 820–829.

[24] B. Zhang, X. Zheng, O. Voznyy, R. Comin, M. Bajdich, M. Garcia-Melchor, L. Han, J. Xu, M. Liu, L. Zheng, F. P. Garcia de Arquer, C. T. Dinh, F. Fan, M. Yuan, E. Yassitepe, N. Chen, T. Regier, P. Liu, Y. Li, P. De Luna, A. Janmohamed, H. L. Xin, H. Yang, A. Vojvodic and E. H. Sargent, *Science*, 2016, **352**, 333–337.

[25] Y. Ling and Y. Li, *Part. Part. Syst. Charact.*, 2014, **31**, 1113–1121.

[26] Y. S. Hu, A. Kleiman-Shwarsctein, A. J. Forman, D. Hazen, J. N. Park and E. W. McFarland, *Chem. Mater*, 2008, **20**, 3803–3805.

[27] A. Kleiman-Shwarsctein, Y. S. Hu, A. J. Forman, G. D. Stucky and E. W. McFarland, *J. Phys. Chem. C*, 2008, **112**, 15900–15907.

[28] T. Odedairo, X. Yan, X. Yao, K. Ostrikov and Z. Zhu, *Adv. Mater.*, 2017, **29**, 1703792.